Journal Name

COMMUNICATION

Surface Patterning of Polyacrylamide Gel Using Scanning Electrochemical Cell Microscopy (SECCM)†

Received 00th January 20xx,
Accepted 00th January 20xx

DOI: 10.1039/x0xx00000x

www.rsc.org/

Elizabeth E. Oseland,[a] Zoë J. Ayres,[a] Andrew Basile,[a,b] David M. Haddleton,[a] Paul Wilson*[a] and Patrick R. Unwin*[a]

Scanning electrochemical cell microscopy is introduced as a new tool for the synthesis and deposition of polymers on SAM-functionalised Au surfaces. The deposition of poly(*N*-hydroxyethyl acrylamide) is shown to be enhanced through the electrochemical generation of activating Cu(I)Cl/Me_6TREN catalyst. Initiation of the polymerisation reaction is most likely due to *in situ* generation of reactive oxygen species following oxygen reduction.

The functionalization of surfaces with patterned polymer structures is currently of high interest[1-4] and is commonly achieved using methods such as photolithography,[5] block copolymer self-assembly[6] and induction of chemical instability.[7] Although these techniques are useful for the mass-production of materials, probe-based techniques can offer distinct design capability when fabricating unique, intricate structures. Examples of probe-based methods include ink-jet printing,[8] dip-pen lithography,[9] polymer pen lithography,[10] electrospinning[11] and scanning electrochemical microscopy.[12] Techniques have also been developed to fabricate structures on a substrate through controlled contact between a surface and a probe-meniscus.[13] Meniscus-based methods tend to employ single-barrelled pipette probes; however, the resulting lack of a feedback protocol for probe positioning can be restrictive in terms of the number of points of contact that can be made with the surface and possible tip crash. In light of these drawbacks, dual-barrel meniscus-based pipette probes have been developed to provide positional feedback between the probe meniscus and surface.[14, 15] The dual-barrel approach employed in scanning electrochemical cell microscopy (SECCM) offers a combination of well-controlled lateral movement and positional feedback of the probe that has been exploited in recent studies for microscale and nanoscale electrochemical patterning of surfaces.[16-19]

This paper considers the possibility of using SECCM as a tool to carry out local polymer synthesis in the meniscus, as exemplified by McKelvey *et al*,[17] to pattern functional vinyl polymer structures on a surface. To some extent, our work takes the idea of electrochemically mediated atom transfer radical polymerisation (eATRP)[20] on a local scale with a moveable probe for the preparation of discretely functional surfaces. Surfaces functionalised with polyacrylamide brushes have a wide range of applications in the field of biotechnology such as inhibition of non-specific fouling, protein separation, cell adsorption and drug encapsulation.[21]

Electrochemically mediated surface initiated ATRP (SI-eATRP) has been explored in bulk reactions[22-26] but it has never been attempted using a meniscus-based method like SECCM. In this study, the polymerisation of *N*-hydroxyethyl acrylamide on gold surfaces covered with self-assembled monolayers (SAMs) is reported. SI-eATRP in bulk solution has already been used to form polyacrylamide brushes on gold electrodes for Pb^{2+} sensing, however this was at elevated temperature and over a timescale of 1.5 hours.[27] In contrast, we draw on recent advances in reaction conditions that allow the rapid polymerisation of acrylamides in aqueous solution.[28, 29]

Initially, gold substrates were functionalised with bis[2-(2-bromoisobutyryloxy)ethyl] disulfide (Br_{SAM}) to present *a*-bromoester initiating groups. Polymer deposition experiments were carried out with the aim of forming poly(HEAA) brushes through SI-eATRP, upon contact of the meniscus from the probe with the surface, via the electrochemical generation of activating Cu(I)Cl/Me_6TREN from Cu(II)Cl/Me_6TREN precatalyst within the tip. Experiments were also attempted under argon, in a sealed environmental cell, to prevent inhibition by detrimental side reactions taking place between the growing polymer chains and excessive levels of molecular oxygen. Dual barrel borosilicate glass theta pipettes were filled with a deaerated aqueous solution containing *N*-hydroxyethyl acrylamide (HEAA) monomer, $CuCl_2$ and Me_6TREN (full details in Section S1, ESI†). Ag|AgCl quasi reference counter electrodes (QRCEs) were then inserted into each barrel, with a potential

[a] Department of Chemistry, University of Warwick, Gibbet Hill Road, Coventry, CV4 7AL, UK. Email: p.wilson.1@warwick.ac.uk, p.r.unwin@warwick.ac.uk
[b] Institute for Frontier Materials, Deakin University, Geelong, VIC 3216, Australia
† Electronic Supplementary Information (ESI) available. See
DOI: 10.1039/x0xx00000x

difference, V_{bias} of -100 mV applied between them to induce an ion conductance current, i_{barrel} (see Figure 1A). For positional feedback, the probe position was oscillated normal to the surface (±50 nm amplitude). This induced an alternating current component of the ion conductance current ($i_{barrel\ AC}$), which could be used as a set point upon contact between the meniscus and surface to prevent tip crash or meniscus detachment during polymer deposition. Polymerisation of HEAA at the interface between the meniscus and surface was initiated via the application of a reducing potential to the substrate (see Figure 1B). Prior to patterning experiments, cyclic voltammetry (CV) was used to find a suitable reducing potential (see Figure 1C). A $V_{surface}$ potential of -0.55 V was applied during all poly(HEAA) patterning experiments to ensure efficient turnover of the inactive Cu^{2+} species to the active Cu^{+} species (and the reduction of trace O_2; *vide infra*).

To pattern poly(HEAA) using SECCM, the position and time that the meniscus was in contact with the surface was closely controlled. The pipette was brought down to the surface at a speed of 250 nm s^{-1} until the meniscus just contacted the surface, inducing an increase in AC barrel current magnitude ($i_{barrel\ AC}$) that was used as a set point to keep the meniscus in contact with the surface for a set time period. While the pipette was in contact with the surface, the probe position, surface current ($i_{surface}$), barrel ion-conductance current (i_{barrel}) and $i_{barrel\ AC}$ were all monitored and recorded (see Figure 2A i-iv) giving exquisite control over the reaction and deposition. The scheme of the probe in Figure 2A shows the relationship between the pipette position and movement, and the corresponding SECCM response during poly(HEAA) deposition. During region 1, the pipette meniscus is not in contact with the surface and only a small barrel ion-conductance current is observed (Figure 2A(iii)). At point 2, the meniscus comes into contact with the surface and both the AC and DC barrel currents (Figures 2A(iii) and 2A(iv)) significantly increase due to the change in meniscus geometry.[15]

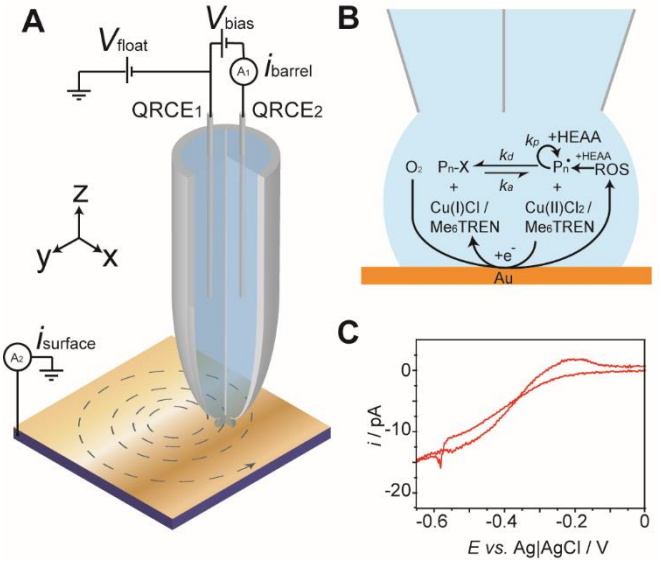

Fig. 1 (A) Illustration of the SECCM setup used for polymer deposition. The surface electrode was held at a potential of -0.55 V to induce polymerisation of HEAA at the interface between the surface and tip meniscus. (B) Mechanism for HEAA polymerisation at the electrode surface, where a reactive oxygen species initiator (ROS) is produced by the electrochemical reduction of oxygen. (C) CV (100 mV s^{-1}) using the SECCM setup under argon (1 µm diameter pipette) on Au/Br_{SAM} using 2 mM $CuCl_2$/Me_6TREN and 1 M HEAA.

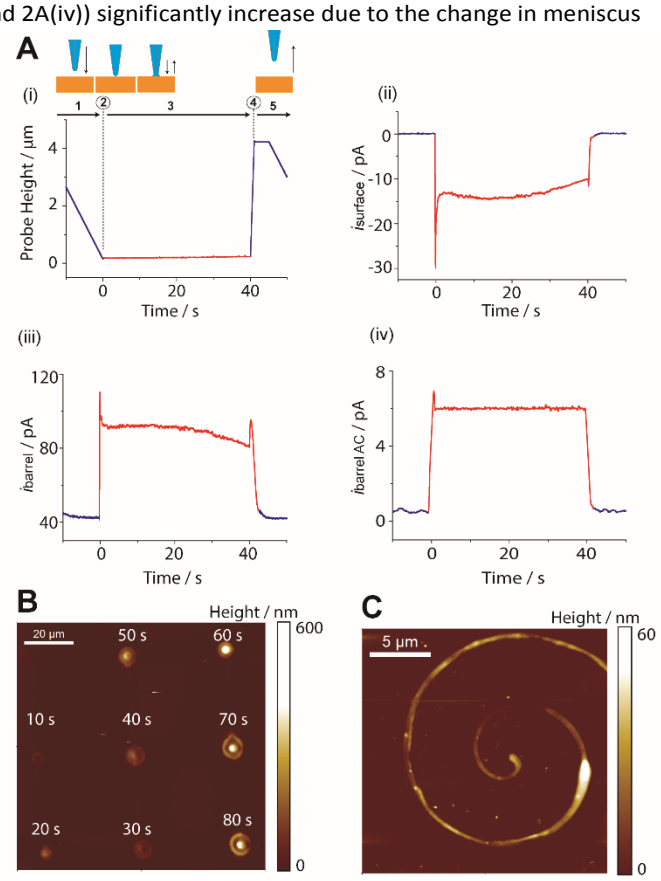

Fig. 2 (A) Typical SECCM responses during a 40 second deposition of poly(HEAA) including (i) probe height, (ii) surface current, (iii) barrel ion-conductance current and (iv) AC barrel current magnitude. Diagrams have been placed above to show the relationship between probe movement and the various current responses. (B) AFM image of an array of poly(HEAA) deposits on a Au/Br_{SAM} surface formed by SECCM denoting deposition time above each feature. (C) AFM image of a poly(HEAA) spiral formed using fast-scanning SECCM.

Current begins to flow through the surface (Figure 2A(ii)) due to the reduction of $Cu(II)Cl_2$/Me_6TREN to Cu(I)Cl/Me_6TREN. During region 3, the pipette meniscus is held on the surface for the desired duration of poly(HEAA) deposition. The slight decrease in both surface and barrel ion conductance currents suggests that HEAA polymerisation will reduce current flow. This can be attributed to both an increase in solution viscosity and surface passivation by adsorption of poly(HEAA) to the surface. At point 4, the pipette is retracted a distance of 4 µm before being laterally moved during region 5 at a speed of 10 µm s^{-1} to the next deposition spot.

Initial patterning experiments involved using a 1 µm diameter pipette to form grid structures by depositing poly(HEAA) at evenly spaced points over incrementally increasing timescales (Figure 2B). Poly(HEAA) deposits increased in height with increasing deposition time, indicating increasing monomer conversion with length of applied activation potential. Control experiments using an applied $V_{surface}$ of -0.15 V showed no deposition, ascertaining that poly(HEAA), as opposed to monomer HEAA, was being deposited. To explore the capability of SECCM for deposition of

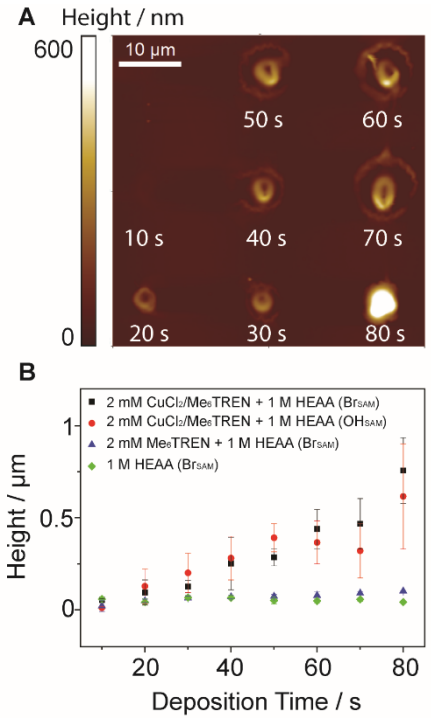

Fig. 3 (A) AFM image of an array of poly(HEAA) deposits on a Au/OH_{SAM} surface formed by SECCM denoting deposition time below each feature. (B) Average peak height of poly(HEAA) deposits formed on Au/Br_{SAM} or Au/OH_{SAM} surfaces during SECCM using a 1 µm diameter pipette containing aqueous solutions of 1 M HEAA with or without Me_6TREN ligand and $CuCl_2$ catalyst.

more complex structures, a LabVIEW program previously developed for high-speed electrochemical imaging[30] was utilised to deposit poly(HEAA) in spiral shapes using a 200 nm diameter pipette (Figure 2C). Polymer deposition was confirmed using X-ray photoelectron spectroscopy, which showed a clear N 1s peak associated with the N-C bond in poly(HEAA), following deposition experiments (details in section S2, ESI†). It was also noted that the Br 3d peak from the SAM decreased after patterning, consistent with a deposited surface layer.

To investigate whether the Au/Br_{SAM} was important for Si-eATRP, a second SAM was prepared that was OH-terminated (Au/OH_{SAM}). Polymer deposition was again observed following repeated grid deposition experiments on the Au/OH_{SAM} surface (Figure 3A). A similar relationship between deposition time and height was observed (Figure 3B).

Optical images of an SECCM tip after deposition experiments revealed a gel-like material protruding from the tip, suggesting at least some polymerisation within the end of the tip (see Figure S2, ESI†).

Polymerisation of HEAA within the tip promoted by HEAA reduction alone was discounted by cyclic voltammetry, which showed no discernible reduction peak for HEAA and Me_6TREN under deaerated solution conditions (see Figure S3, ESI†). It was thus hypothesised that reactive oxygen species formed via reduction of traces of molecular oxygen could provide a source of radicals capable of initiating vinyl polymerisation within the tip. To test this idea, CVs were initially collected using the SECCM setup under aerated and deaerated conditions (Figure 4). Cyclic voltammetry on a clean Au surface using a deaerated KCl solution showed trace oxygen reduction taking place whilst the SECCM system was under argon. However, the magnitude of the oxygen reduction current was more than ten times lower than when using an aerated KCl solution in an aerated SECCM setup.

To establish whether trace molecular oxygen or a product of its reduction initiated HEAA polymerisation, SECCM grid deposition on Au/Br_{SAM} surfaces was carried out under argon using a deaerated 1 M HEAA aqueous solution (see Figure S4, ESI†). A different $V_{surface}$ was applied for each grid deposition, from -0.1 V to -0.4 V. There was no detected deposit at -0.1 V and an increase in the amount deposited with increasing cathodic potential, which implies that the extent of deposition is related to the reduction potential and therefore the nature of oxygen species present. Reactive oxygen species (ROS), such as hydrogen peroxide have been shown to be produced during electrochemical reduction of molecular oxygen in aqueous solutions on gold electrodes.[31, 32] Thus, the extent of oxygen reduction is increased with increasing cathodic potential resulting in a decrease in the trace amount of inhibiting molecular oxygen and an increase in hydrogen peroxide, a well-known initiator for free radical polymerisation.[33] Alternatively, high concentrations of molecular oxygen can inhibit polymerisation via radical addition to propagating polymer chains forming less reactive peroxide radicals.[34] This was exemplified by attempting patterning experiments in the absence of any deaeration. This resulting in no polymer deposition (see Figure S5, ESI†).

Finally, grid depositions were repeated on Au/Br_{SAM} surfaces using aqueous solutions of 1 M HEAA, with systematic removal of the eATRP reagents. Subsequent AFM images of the surfaces verified HEAA polymerisation in the absence of $CuCl_2$ and Me_6TREN (see Figure S6, ESI†). Measurement of the peak height of poly(HEAA) deposited over different timescales highlighted that there was an increase in the degree of HEAA polymerisation when electrochemical generation of CuCl(I)/Me_6TREN was possible (Figure 3B). Furthermore, a linear increase in deposition height with time was observed in the presence of $CuCl_2$/Me_6TREN, which infers that polymerisation initiated by ROS within the tip proceeds with the degree of control associated with the eATRP mechanism.

In summary, we have shown that the dual-barrel SECCM-based meniscus method can be used to pattern poly(HEAA)

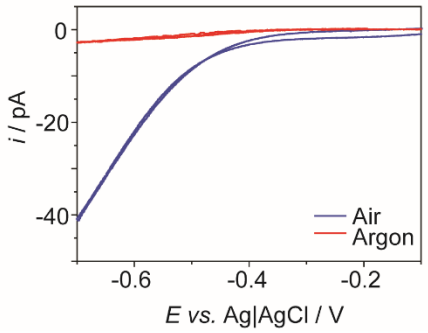

Fig. 4 CVs (50 mV s^{-1}) recorded using the SECCM setup (1.5 µm diameter pipette) under air or argon using an aqueous solution of 20 mM KCl.

films on SAM-functionalised gold surfaces. SI-eATRP occurs due to the presence of trace amounts of oxygen in our setup resulting in polymerisation initiated by ROS formed during electrochemical reduction of trace amounts of molecular oxygen. The extent of ROS generation can be controlled via the applied potential. Furthermore, the enhancement of film deposition following the electrochemical generation of CuCl/Me_6TREN also suggests the importance of a classical eATRP-like mechanism, which takes place concurrently within the pipette. It is envisioned that with refinement of the catalytic system, the SECCM setup will be capable of meniscus-confined SI-eATRP for polymer brush patterning. We also aim to reduce polymer feature size to the nanoscale. This should be achievable by using hydrophobic surfaces to reduce wetting, speeding up lateral movement of the probe (in the case of spiral deposition) and by using smaller diameter SECCM tips.[35]

We thank Ashley Page, Minkyung Kang and Faduma Maddar for helpful discussions, and Emma Ravenhill and Lingcong Meng for substrate preparation. We also thank the Warwick Photoemission Facility. EEO thanks the EPSRC and Syngenta UK for an industrial case award and PW thanks the Leverhulme Trust for an Early Career Fellowship. AB acknowledges the Australian Government's Endeavour Fellowships and Scholarships Programme. This work has been performed, in part, through ARC ACES (insert grant number).

Notes and references

1. Z. Nie and E. Kumacheva, *Nat Mater*, 2008, **7**, 277-290.
2. H. G. Yoo, M. Byun, C. K. Jeong and K. J. Lee, *Adv. Mater.*, 2015, **27**, 3982-3998.
3. J. F. Fennell, S. F. Liu, J. M. Azzarelli, J. G. Weis, S. Rochat, K. A. Mirica, J. B. Ravnsbæk and T. M. Swager, *Angew. Chem. Int. Ed.*, 2016, **55**, 1266-1281.
4. M. Verhulsel, M. Vignes, S. Descroix, L. Malaquin, D. M. Vignjevic and J.-L. Viovy, *Biomaterials*, 2014, **35**, 1816-1832.
5. B. Li, M. He, L. Ramirez, J. George and J. Wang, *ACS Applied Materials & Interfaces*, 2016, **8**, 4158-4164.
6. L. Shen, C. He, J. Qiu, S.-M. Lee, A. Kalita, S. B. Cronin, M. P. Stoykovich and J. Yoon, *ACS Applied Materials & Interfaces*, 2015, **7**, 26043-26049.
7. J. J. S. Rickard, I. Farrer and P. Goldberg Oppenheimer, *ACS Nano*, 2016, **10**, 3865-3870.
8. A. Garcia, N. Hanifi, B. Jousselme, P. Jégou, S. Palacin, P. Viel and T. Berthelot, *Adv. Funct. Mater.*, 2013, **23**, 3668-3674.
9. M. Guardingo, P. González-Monje, F. Novio, E. Bellido, F. Busqué, G. Molnár, A. Bousseksou and D. Ruiz-Molina, *ACS Nano*, 2016, **10**, 3206-3213.
10. F. Huo, Z. Zheng, G. Zheng, L. R. Giam, H. Zhang and C. A. Mirkin, *Science*, 2008, **321**, 1658-1660.
11. J. Lee, S. Y. Lee, J. Jang, Y. H. Jeong and D.-W. Cho, *Langmuir*, 2012, **28**, 7267-7275.
12. F. Hauquier, T. Matrab, F. Kanoufi and C. Combellas, *Electrochim. Acta*, 2009, **54**, 5127-5136.
13. J. T. Kim, S. K. Seol, J. Pyo, J. S. Lee, J. H. Je and G. Margaritondo, *Adv. Mater.*, 2011, **23**, 1968-1970.
14. K. T. Rodolfa, A. Bruckbauer, D. Zhou, A. I. Schevchuk, Y. E. Korchev and D. Klenerman, *Nano Lett.*, 2006, **6**, 252-257.
15. N. Ebejer, M. Schnippering, A. W. Colburn, M. A. Edwards and P. R. Unwin, *Anal. Chem.*, 2010, **82**, 9141-9145.
16. P. M. Kirkman, A. G. Güell, A. S. Cuharuc and P. R. Unwin, *J. Am. Chem. Soc.*, 2013, **136**, 36-39.
17. K. McKelvey, M. A. O'Connell and P. R. Unwin, *Chem. Commun.*, 2013, **49**, 2986-2988.
18. H. V. Patten, L. A. Hutton, J. R. Webb, M. E. Newton, P. R. Unwin and J. V. Macpherson, *Chem. Commun.*, 2015, **51**, 164-167.
19. A. N. Patel, K. McKelvey and P. R. Unwin, *J. Am. Chem. Soc.*, 2012, **134**, 20246-20249.
20. A. J. D. Magenau, N. C. Strandwitz, A. Gennaro and K. Matyjaszewski, *Science*, 2011, **332**, 81-84.
21. C. J. Fristrup, K. Jankova and S. Hvilsted, *Soft Matter*, 2009, **5**, 4623-4634.
22. B. Li, B. Yu, W. T. S. Huck, F. Zhou and W. Liu, *Angew. Chem.*, 2012, **124**, 5182-5185.
23. Y. Hu, G. Yang, B. Liang, L. Fang, G. Ma, Q. Zhu, S. Chen and X. Ye, *Acta Biomaterialia*, 2015, **13**, 142-149.
24. J. Yan, B. Li, B. Yu, W. T. S. Huck, W. Liu and F. Zhou, *Angew. Chem. Int. Ed.*, 2013, **52**, 9125-9129.
25. N. Shida, Y. Koizumi, H. Nishiyama, I. Tomita and S. Inagi, *Angew. Chem. Int. Ed.*, 2015, **54**, 3922-3926.
26. L. T. Strover, J. Malmström, L. A. Stubbing, M. A. Brimble and J. Travas-Sejdic, *Electrochim. Acta*, 2016, **188**, 57-70.
27. Y. Sun, H. Du, Y. Deng, Y. Lan and C. Feng, *J. Solid State Electrochem.*, 2016, **20**, 105-113.
28. P. Chmielarz, S. Park, A. Simakova and K. Matyjaszewski, *Polymer*, 2015, **60**, 302-307.
29. G. R. Jones, Z. Li, A. Anastasaki, D. J. Lloyd, P. Wilson, Q. Zhang and D. M. Haddleton, *Macromolecules*, 2016, **49**, 483-489.
30. D. Momotenko, J. C. Byers, K. McKelvey, M. Kang and P. R. Unwin, *ACS Nano*, 2015, **9**, 8942-8952.
31. J. C. Byers, A. G. Güell and P. R. Unwin, *J. Am. Chem. Soc.*, 2014, **136**, 11252-11255.
32. G. Gotti, K. Fajerwerg, D. Evrard and P. Gros, *Electrochim. Acta*, 2014, **128**, 412-419.
33. J. L. Pradel, B. Boutevin and B. Ameduri, *J. Polym. Sci., Part A: Polym. Chem.*, 2000, **38**, 3293-3302.
34. V. A. Bhanu and K. Kishore, *Chem. Rev.*, 1991, **91**, 99-117.
35. A. G. Güell, A. S. Cuharuc, Y.-R. Kim, G. Zhang, S.-y. Tan, N. Ebejer and P. R. Unwin, *ACS Nano*, 2015, **9**, 3558-3571.